The optic nerve lamina region is a neural progenitor cell niche

S. L. Bernstein[a,b,1], Y. Guo[a], C. Kerr[c], R. J. Fawcett[a], J. H. Stern[d], S. Temple[d], and Z. Mehrabian[a]

[a]Department of Ophthalmology and Visual Sciences, University of Maryland School of Medicine, Baltimore, MD 21201; [b]Department of Anatomy and Neurobiology, University of Maryland School of Medicine, Baltimore, MD 21201; [c]Division of Aging Biology, National Institutes of Health, Bethesda, MD 20892; and [d]Age-Related Macular Degeneration Program, Neural Stem Cell Institute, Rensselaer, NY 12144

Edited by Constance L. Cepko, HHMI and Department of Genetics, Harvard Medical School, Boston, MA, and approved June 26, 2020 (received for review February 4, 2020)

Retinal ganglion cell axons forming the optic nerve (ON) emerge unmyelinated from the eye and become myelinated after passage through the optic nerve lamina region (ONLR), a transitional area containing a vascular plexus. The ONLR has a number of unusual characteristics: it inhibits intraocular myelination, enables postnatal ON myelination of growing axons, modulates the fluid pressure differences between eye and brain, and is the primary lesion site in the age-related disease open angle glaucoma (OAG). We demonstrate that the human and rodent ONLR possesses a mitotically active, age-depletable neural progenitor cell (NPC) niche, with unique characteristics and culture requirements. These NPCs generate both forms of macroglia: astrocytes and oligodendrocytes, and can form neurospheres in culture. Using reporter mice with SOX2-driven, inducible gene expression, we show that ONLR-NPCs generate macroglial cells for the anterior ON. Early ONLR-NPC loss results in regional dysfunction and hypomyelination. In adulthood, ONLR-NPCs may enable glial replacement and remyelination. ONLR-NPC depletion may help explain why ON diseases such as OAG progress in severity during aging.

optic nerve | lamina | neural progenitor cell niche | eye | postnatal axon growth

The human and rodent optic nerve (ON) connecting the eye and brain grows by 80% postnatally (1, 2). Unmyelinated retinal ganglion cell (RGC) axons originating in the retina pass through the optic nerve lamina region (ONLR), the most anterior portion of the optic nerve, before myelination occurs in the more distal portion of the optic nerve (ON) (3). However, the precise sites of postnatal RGC axonal growth and the mechanism by which myelination occurs at sites of newly formed axonal membrane late in postnatal growth are obscure (4).

The ONLR's known properties include inhibiting retinal myelination (5, 6), phagocytic astrocytes (7), and reduced aquaporin-4 (AQP4) levels relative to its surround (8). The ONLR also possesses a vascular plexus with a complexity greater than that of the associated ON (9–11). The ONLR thus comprises a unique region enabling appropriate responses to complex microenvironmental changes.

Adult neural progenitor cells (aNPCs) can reside in niches which have unique regional characteristics, including a vascular plexus (12, 13), reduced relative levels of aquaporin-4 (AQP4) (14), and coexpression of NPC marker proteins, including fibrillar nestin, GFAP, and the Sry box 2 (SOX2) transcription factor (15, 16). CNS-aNPCs act primarily as a reservoir for glial cell replacement in young and mature animals, but can occasionally produce neurons (17, 18). Cultured aNPCs can form neurospheres in low adhesion, serum-free medium (19).

Adult mammalian ONs contain resident SOX2(+)/NG2(+) oligodendrocyte precursors (OPCs) scattered throughout the ON (20). While OPCs largely give rise to replacement oligodendrocytes, OPCs themselves are a largely quiescent cell population that rarely undergoes cell division (20).

Our study demonstrates that apart from typical OPCs in the distal ON, a distinct cell population resides in the ONLR with aNPC properties. ONLR-aNPCs express SOX2 protein and NPC-specific proteins not seen in OPCs, including nestin and GFAP, while lacking the OPC marker protein NG2 (21–25). Using a multifactorial approach, we demonstrate that the postnatal ONLR-NPC niche can generate all macroglial cell forms in the ON, contributing to normal postnatal ON growth, myelination, and cellular replacement.

Results

ONLR Structure Is Consistent with an NPC Niche. The mammalian ONLR in humans and rodents presents as a narrow band of unmyelinated tissue bordering the retina and ON (Fig. 1*A*). Two-photon microscopy of fluorescein-bound gelatin-filled ONLR vessels reveals that these form a vascular plexus with contributions from retina (Ret) and optic nerve (ON) (Fig. 1*B*), as well as from the choroid (26). AQP4 is present at reduced levels in aNPC niches (14). ONLR-AQP4 expression levels are reduced (Fig. 1*C*, in green), compared with either retina or distal ON (Fig. 1*C*, Retina and ON).

While no consistent protein expression pattern exists for aNPCs (27), aNPCs typically express both nestin and SOX2 (21, 28, 29), GFAP, and aldolase dehydrogenase 1L1(Aldh1L1) (30). We defined the mouse and rat ONLR by the absence of myelin,

Significance

The optic nerve lamina region (ONLR) transitions between the eye and optic nerve (ON) and is the primary damage site in the age-related disease open angle glaucoma (OAG). The ONLR inhibits intraocular myelination and enables postnatal ON myelination of growing retinal ganglion cell axons. We show that the ONLR contains an adult neural progenitor cell (NPC) niche capable of generating all macroglial cell types for the anterior ON. Early ONLR-NPC loss causes regional dysfunction and myelination defects. Age-related depletion may help explain development of ON diseases such as OAG.

Author contributions: S.L.B. and Z.M. designed research; S.L.B., Y.G., C.K., R.J.F., S.T., and Z.M. performed research; S.L.B., C.K., and S.T. contributed new reagents/analytic tools; S.L.B., Y.G., C.K., J.H.S., S.T., and Z.M. analyzed data; S.L.B. wrote the paper; and initial research of S.L.B. was performed within J.H.S. and S.T. laboratories.

Competing interest statement: Methods of treating optic nerve diseases using neural progenitor cell growth factors patent application submitted USPTO PCT/US19/16303 01-Feb-2019.

This article is a PNAS Direct Submission.

Data deposition: Data have been deposited in Figshare, https://figshare.com/s/2c75b304e2ed05a37415, with the following accession numbers: 10.6084/m9.figshare.12250223; 10.6084/m9.figshare.12250232; 10.6084/m9.figshare.12250241; 10.6084/m9.figshare.12251945; 10.6084/m9.figshare.12251957.

[1]To whom correspondence may be addressed. Email: sbernstein@som.umaryland.edu.

This article contains supporting information online at https://www.pnas.org/lookup/suppl/doi:10.1073/pnas.2001858117/-/DCSupplemental.

First published July 28, 2020.

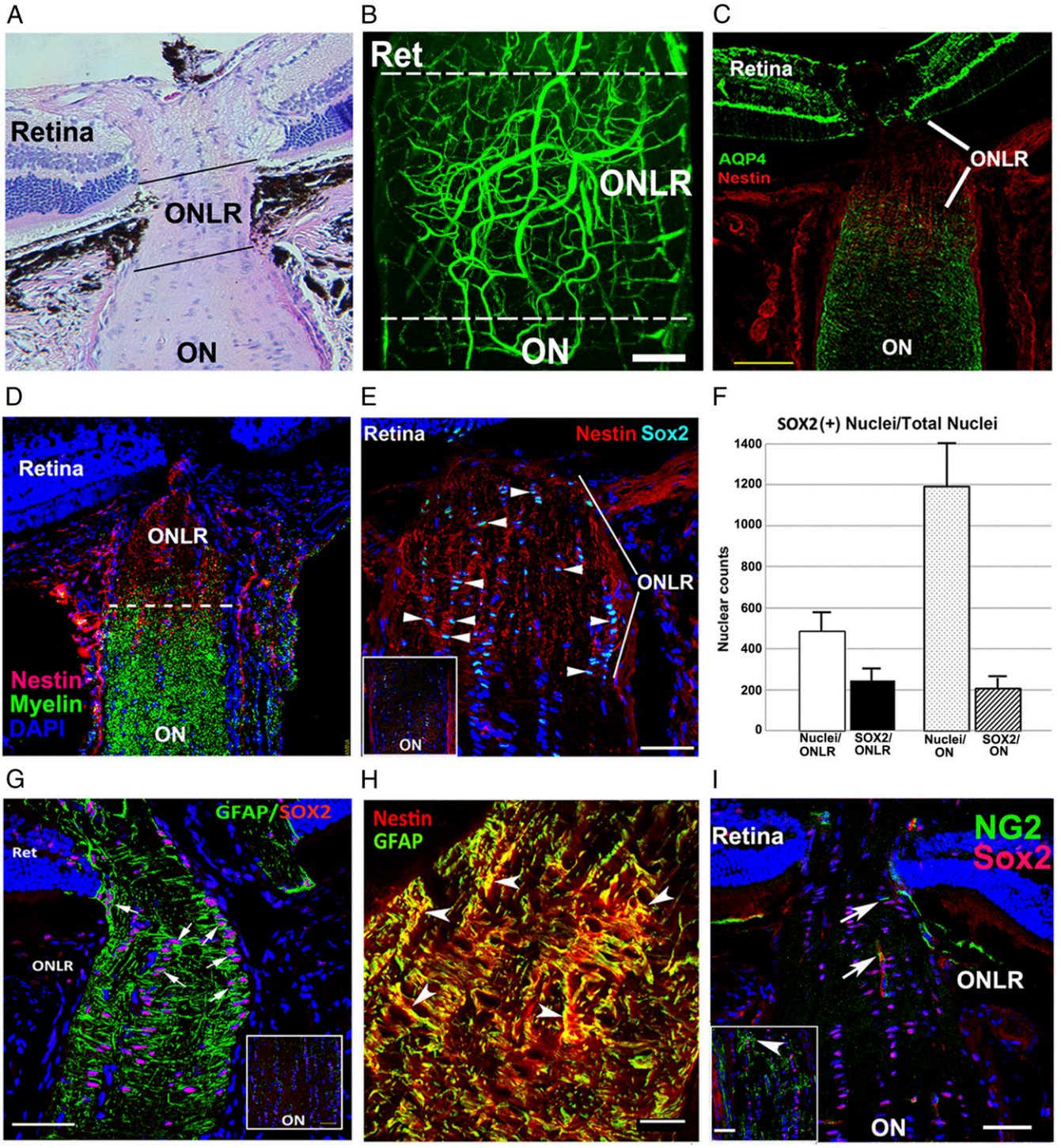

Fig. 1. Rodent ONLR characterization. (*A*) H&E longitudinal section, mouse ONLR. (*B*) Two-photon micrograph of fluorescein-filled rodent (rat) ONLR vessels. ONLR vasculature forms a plexus with contributions from retina (Ret) and ON. (*C*) AQP4 expression in the retina, ONLR, and ON. AQP4 (in green)/Nestin (in red). There is reduced ONLR-AQP4, compared with retina or distal ON. (*D*) Nestin localization in the ONLR. Nestin (red)/myelin (O_4 antibody; green) localization define the ONLR. Nestin expression declines anterograde, with early oligodendrocyte development only below the ONLR. (*E*) Increased SOX2 expression in the ONLR. SOX2(+) nuclei are qualitatively increased in the nestin-enriched ONLR (arrowheads), and present in reduced numbers in the distal ON (Fig. 1 *G*, *Inset*: ON). (*F*) SOX2 nuclear quantification in ONLR and ON. ONLR is enriched in SOX2 nuclei, in terms of both area (*Left* bars), and SOX2:total nuclei (*Right* bars). (*G*) ONLR-SOX2/GFAP expression. GFAP surrounds SOX2(+) nuclei, suggesting that ONLR SOX2(+) cells express both proteins. Distal ON (*Inset*) reveals that cells with SOX2(+) nuclei lack GFAP expression. (*H*) Nestin and GFAP colocalize in the ONLR. Red: Nestin; green: GFAP. (Scale bar: 20 μm.) (*I*) NG2(+)/Sox2(+) OPCs are present only distal to the mouse ONLR. NG2(+) OPCs (green) are only seen in the anterior ON below the ONLR. NG2(+) capillaries/(arrow) are present in the ONLR. *Inset*: NG2(+) cells have a Sox2(+) nucleus (in red). (Scale bar in *H*: 20 μm; *C*, *E*, and *G*: 50 μm; *I*: 100 μm; and *Inset* in *I*: 50 μm.)

using the oligodendrocyte- and OPC-specific O_4 antibody (Fig. 1*D*, in green). ONLR expressed highest levels of nestin relative to other ocular regions (Fig. 1*D*). Filamentous nestin was localized to the ONLR (Fig. 1*D*, in red). Rodent ONLR also coexpressed SOX2(+) nuclei and nestin (Fig. 1*E*, arrowheads) while the distal ON does not (Fig. 1 *E*, *Inset*; compare with

ONLR). Nuclear quantification revealed that ∼50% of mouse ONLR cells express SOX2(+) (247 ± 31.8 vs. 486 ± 41.6 SEM; $n = 3$), compared with ∼17% of distal ON cells (207 ± 17.9 vs. 1193 ± 127 SEM; $n = 3$; Fig. 1*F*; compare ONLR and ON). GFAP is another NPC marker (16) and is expressed in many ONLR cells (Fig. 1*G*, arrows), and coexpressed with ONLR-nestin (Fig. 1*H*). Hence, the ONLR includes numerous cells coexpressing these three characteristic markers of adult NPCs.

ONLR SOX2(+) cells are largely NG2(−) in the rat and mouse (Fig. 1*I*, ONLR) and thus are not oligodendrocyte progenitor cells (OPCs). NG2(+)/SOX2(+) OPCs are detectable throughout the ON below the ONLR in the growing mouse (25 d) ON (*Inset*, arrowheads, Fig. 1*I*). Since NPCs do not express NG2 but do express GFAP, nestin, and SOX2, this pattern of expression suggests that ONLR-resident SOX2(+) cells are distinct from SOX2(+)/NG2(+) OPCs.

ONLR-NPCs: Transgenic Confirmation. We confirmed in vivo SOX2 expression in ONLR and ONs in transgenic reporter mouse strains. Currently available transgenic animals with nestin-cre constructs (31), did not generate ON or ONLR signals, possibly due to multiple expression variables (32). We therefore utilized crosses between a transgenic mouse reporter strain expressing Cre under control of the SOX2 promotor, which was further restricted by addition of an ER2 receptor cassette enabling activation only after administration of tamoxifen (TAM) or its active metabolite 4 hydroxytamoxifen (4OHT). This transgene is referred to as SOX2-Cre. This construct enabled us to selectively localize postnatal SOX2 activity, but because the ER2 cassette regulates available Cre activity, cells with higher SOX2-Cre expression levels activated with TAM or 4OHT would be expected to induce recombination events more rapidly than cells with lower Cre-expression levels.

SOX2-Cre-ER2 mice were crossed with the ROSA26 td-Tomato-loxP (EGFP) reporter mouse strain, to generate double mutant progeny (referred to as SOX2-GFP). SOX2-GFP mice express GFP in SOX2(+) cells and their descendants only after induction by TAM or 4OHT (Fig. 2*A*), enabling precise identification of the SOX2-expressing cells and their progeny postinduction.

We administered TAM and 4OHT to 19 d postnatal (PN) animals (schematic, Fig. 2*A*). Robust GFP expression was seen in hippocampus 14 d postadministration (Fig. 2*B*). ON-SOX2-GFP expression 14 d post-TAM localized to the ONLR but was indistinct (Fig. 2*C*). A 30 d interval following TAM administration enabled identification of distinct cell patterns (Fig. 2*D*), but also revealed expression in the distal ON, with GFP/NG2 colocalization (Fig. 2 *D*, *Inset*, arrowheads). GFP/TdTomato recombination efficiency in the lamina 30 d postinduction was ∼40% (33). The 30 d post-TAM, ONLR-GFP expression was identifiable in processes transverse to the long axis of the nerve (Fig. 2*D*, ONLR). ONLR-GFP cells were NG2(−) but colocalized with nestin (Fig. 2*E*, arrows). ONLR 30-μm thick cross-section Z-stack reconstructions revealed individual GFP(+) cells (Fig. 2*F*).

GFP expression was also seen below the ONLR in the anterior ON at 30 d in NG2(+) cells consistent with OPCs (Fig. 2*D*, arrows). SOX2-driven GFP expression 30 d postinduction was also present in structures parallel with the long axis of the ON, consistent with axon-myelinating segments (Fig. 2*D*, arrowheads). Below the ONLR, we identified both GFAP(+)/GFP(+) (Fig. 2*G*, arrow) as well as GFP(−)/GFAP(+) (Fig. 2*G*, arrowheads) cells consistent with astrocytic morphology.

We also evaluated GFP and CNPase (a marker for mature oligodendrocyte myelin) colocalization in both the anterior ON and mid-ON areas in the young adult. TAM was administered at 40 d PN (after ON growth is largely over). Tissues were collected 30 d postinduction. GFP colocalized with GFAP and CNPase in the anterior portion of the optic nerve (just below the lamina; see *SI Appendix*, Fig. S1), while farther down in the mid ON, the majority of GFP colocalized with NG2 (OPC marker), with little if any colocalization with CNPase. The majority of astrocytes in the ON are SOX2(−)/GFP(−), suggesting that they likely were generated prior to SOX2-GFP(+) induction. Our data support the hypothesis that ONLR-SOX2/nestin(+) NPCs can give rise postnatally to both NG2(+) OPCs and to mature oligodendrocytes, as well as GFP(+)/GFAP(+) cells with astrocytic morphology.

While GFP expression was strong in the hippocampus of SOX2-GFP animals (Fig. 2*B*), GFP accumulated only slowly in the ONLR and ON at the same time interval (compare Fig. 2*B* with Fig. 2*C*). To identify the role of ONLR-NPCs in postnatal ONLR function, we focused on the effects of SOX2-NPC ablation in the ONLR and ON using double mutant animals constructed with the ER2-SOX2-Cre transgene and a FLOXed diphtheria toxin-A (DTA) gene in the ROSA26 locus (referred to as SOX2-DTA animals). Cre-based recombination induces DTA protein (34), enabling selective deletion of SOX2-expressing cells following tamoxifen administration. SOX2-DTA animals thus provide a highly sensitive tool for analyzing early effects of ONLR-SOX2(+) cell loss, since DTA ablates them. Intraperitoneal (IP) tamoxifen resulted in 100% animal lethality by 10 d postadministration, presumably due to general SOX2 suppression. Local administration of 4OHT via retrobulbar (RB) injection, enabled us to avoid lethality, and enabled selective elimination of SOX2-expressing cells in one eye. We confirmed local administration efficacy using the SOX2-GFP animals (Fig. 2 *C*–*G*). However, we found that RB injection also induced GFP expression in resident intraretinal Sox2(+) cells at 30 d postadministration (*SI Appendix*, Fig. S2). These include SOX2(+) cells with Mueller cell-astrocyte type morphology (*SI Appendix*, Fig. S2, arrows), and CHAT(+) cells that give rise to two GFP(+) synaptic layers in the inner plexiform layer (IPL), representing amacrine neurons (*SI Appendix*, Fig. S2*A*, arrowheads, and compare with *SI Appendix*, Fig. S2*B*, arrows and arrowheads).

We compared ON morphology in SOX2-DTA mice subjected to 4OHT and contralateral injections with vehicle (Kolliphor), 14 d and 30 d postadministration. Ocular tissues were compared for size and appearance (Fig. 3*D*). ONLRs from SOX2-DTA animals treated with vehicle and 4OHT were also evaluated for ONLR nestin (Fig. 3 *A* and *B*) and quantified for SOX2 nuclei (Fig. 3*C*). ON ultrastructure was examined and quantified using transmission electron microscopy (TEM) (Fig. 3 *E*–*J*). The number of SOX2(+) nuclei in 4OHT nerves was reduced as compared to the contralateral vehicle, which was similar to wild type (WT) (Fig. 3*C*).

Nerves of SOX2-DTA animals given vehicle were normal appearing in terms of both diameter and myelination (Fig. 3*D*, Veh), with a normal contralateral optic tract (OT) (Fig. 3*D*). In contrast, 4OHT-treated ONs and ipsilateral OTs 14 d postinduction varied widely, ranging from mildly reduced in diameter to hypoplastic (Fig. 3*D*, compare Veh and 4OHT). Severe hypoplasia was observed in 2/22 RB-injected animals, likely associated with injection-associated intraorbital damage. These latter animals were excluded from the study.

4OHT-treated nerves from SOX2-DTA animals exhibited selective loss of nestin (Fig. 3*B*, nestin, compared with vehicle-treated nerve) (Fig. 3*A*). There was also a loss of SOX2(+) nuclei. Quantification of SOX2(+) nuclei at 4 d post-RB-4OHT administration in SOX2-DTA animals revealed a loss of over 2/3 of SOX2 nuclei in the ONLR compartment, compared with WT animals treated with 4OHT [Fig. 3*C*, 6.9 ± 1.9% SOX2(+) nuclei vs. 21.8 ± 4.9% in WT-ONLR; $n = 3$ animals group, ±SEM]. These data suggest that the loss of SOX2(+) nuclei postinduction is not due simply to tamoxifen-related drug toxicity or RB injection, but rather a loss of NPCs.

The ONLR extends ∼300 μm from the globe in 60 d PN mouse eyes (ref. 35 and Fig. 1). We hypothesized that one role for ONLR-NPCs was to enable unidirectional myelination of the growing postnatal RGC axon as it emerges from the ONLR, by supplying ONLR-NPC-derived macroglia. In this case, active

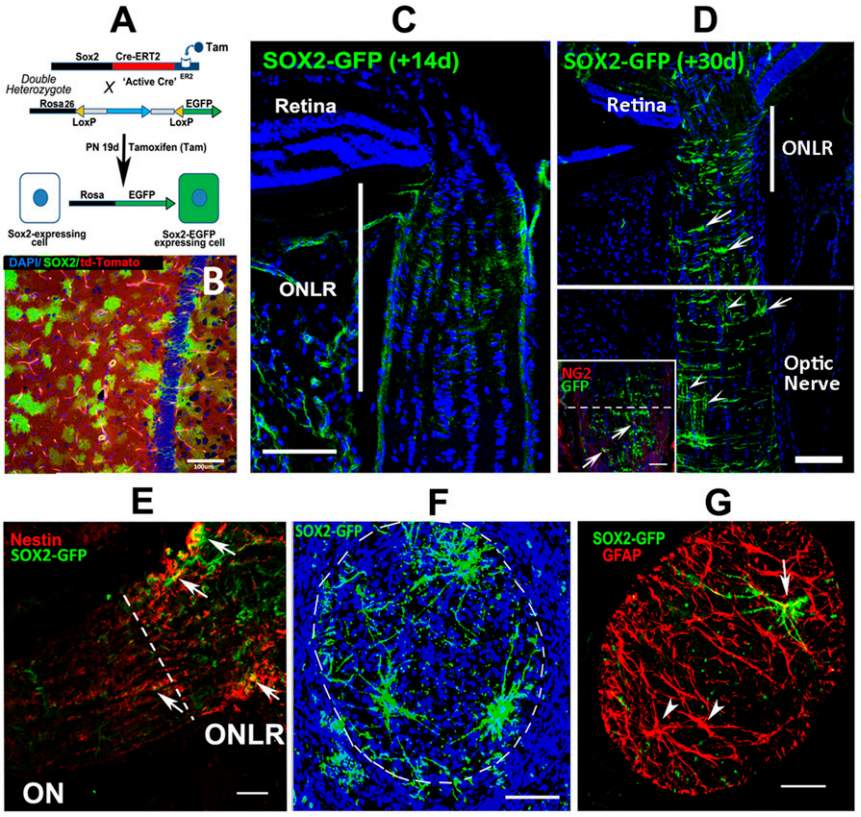

Fig. 2. GFP induction patterns in SOX2-Cre reporter mice. (*A*) Schematic of 4OHT/tamoxifen induction in 19 d PN SOX2-GFP mice. The unrecombined ROSA26 locus constitutively expresses td-Tomato (red cytoplasm; background cells in *B*). Tamoxifen enables Cre recombinase expression in SOX2-expressing cells, with recombined cells expressing GFP expression in parents and their progeny. Mice were injected systemically (IP) with tamoxifen or locally (retrobulbar) with 4OHT. Tissues were collected either at 14 d postinduction (33 d postnatal brain; B and ONLR; *C*), or 30 d (50 d postnatal; D). (*B*) Hippocampal GFP expression 14 d postinduction. GFP(+) cells are present on a red (td-Tomato) background. (*C*) ONLR-SOX2-driven GFP expression 14 d postinduction. GFP expression is low, and limited to the ONLR. (*D*) ONLR SOX2-driven GFP expression 30 d postinduction. *Inset*: GFP is present in short processes parallel to the long axis of the ON, corresponding to myelin segments (arrowheads). (*E*) SOX2-GFP expression is clustered in ONLR-nestin(+) cells (arrows). GFP expression is present in ONLR and in the anterior ON. (*F*) Thirty-micrometer Z-stack ONLR cross-section in a SOX2-GFP animal 30 d postinduction. (*G*) ONLR-GFP expression is concentrated in large GFAP(+) cells with a stellate morphology. (Scale bar in *G*: 50 μm; all other photos: 100 μm.)

anterior myelination in the growing ON should occur focally as a distinct zone directly below the ONLR, as unmyelinated axons emerge from the eye. We compared myelination patterns in SOX2-DTA mice treated with 4OHT in the anterior- and mid-ON in which active ON growth was still occurring (Fig. 3 *E*–*J*). Mice were treated at 19 d PN and evaluated at 33 d PN (14 d post-treatment). ONs were ultrastructurally analyzed using TEM at their anterior (1.5 to 2 mm from eye) and distal (5 mm from the eye) segments. Prior to this assay, we analyzed 4OHT RB-injection toxicity in WT animals (10 to 60 mg/mL). Concentrations of 30 mg/mL 4OHT in WT animals showed no gross alterations or significant axonal loss (*SI Appendix*, Fig. S3). A similar result was seen in SOX2-DTA animals treated with vehicle (Fig. 3 *F* and *H*). Occasional abnormal axons (arrow, *SI Appendix*, Fig. S3*D*) were identifiable in all untreated and treated nerves up to 60 mg/mL 4OHT, with no significant differences between treatment groups (quantified in *SI Appendix*, Fig. S3*E*).

ON ultrastructure was examined by measuring axonal diameter and myelination using TEM (Fig. 3 *E*–*J*). Relative myelin thickness to axon diameter (G ratio) was unchanged and similar at both anterior (Fig. 3*F*) and distal segments (Fig. 3*H*) in SOX2-DTA vehicle-treated animals. In contrast, 4OHT-treated nerves of SOX2-DTA animals revealed axonal hypomyelination in the anterior ON segment (Fig. 3*E*), with a corresponding increase in the G ratio (black bar, Fig. 3*J* ONLR; compare with white bar, vehicle-treated nerve).

Mean overall axon diameter in the anterior segments of 4OHT- vs. vehicle-treated nerves showed a nonsignificant trend toward larger axon diameters (Fig. 3*I* ONLR; compare vehicle, 522 ± 190 nm vs. 4OHT, 771 ± 382 nm SD). There was no significant difference in mean axon diameter from the distal ON segments of both treatment groups (607 ± 261 nm for vehicle vs. 612 ± 228 nm SD for 4OHT; $P = 0.859$; two-tailed t test) and a similar packing density.

We calculated the mean G ratio for axons in vehicle- and 4OHT-treated nerves, at both anterior and posterior regions (Fig. 3*J*). 4OHT treatment resulted in a mean increase in the G ratio of the anterior nerve, indicating relatively thinner myelin sheaths in the anterior axonal region compared with vehicle-treated nerves from the same animals (Fig. 3*J*; ONLR: 4OHT = 0.77 ± 0.04 vs. vehicle = 0.67 ± 0.02 SD). This was significant ($P < 0.001$, two-tailed t test). This was not apparent in the distal segment; the mean distal ON G ratio for 4OHT- and vehicle-treated nerves (Fig. 3*J*: ON. 4OHT; 0.69 ± 0.08 vs. vehicle; 0.66 ± 0.09 SD) from the same animal(s) was nonsignificant ($P > 0.05$; two-tailed t test). The ON G-ratio data for 33-d animals is lower than that reported for mature (60-d-old) WT animals (36).

The anterior ON of 4OHT-treated nerves also had a trend toward increased axon packing density (decreased distance between axons), in the anterior portion of 4OHT treated- compared with vehicle-treated nerves from the same animals (Compare axonal packing in Fig. 3*E*; 4OHT treated, with

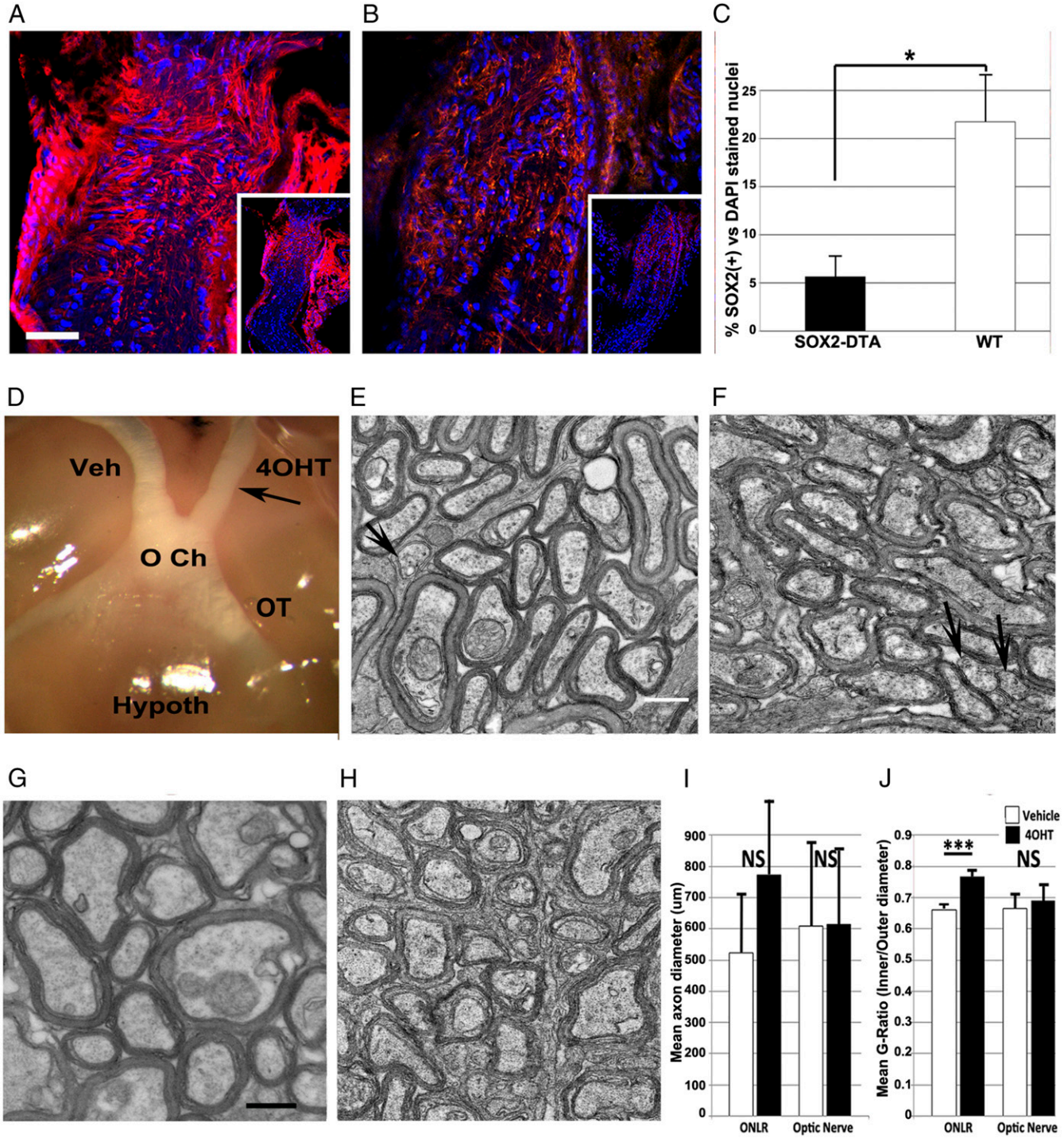

Fig. 3. Late postnatal deletion of SOX2(+)/Nestin(+) ONLR-NPCs affects postnatal ON growth and myelination. (*A–C*) Immunohistological analysis: (*A*) Nestin expression in WT mice post-4OHT injection. *Inset*: low power view showing nestin is concentrated in the ONLR. (*B*) Reduced ONLR nestin expression following 4OHT. (*C*) SOX2 expression is reduced in the ONLR of 4OHT-induced SOX2-DTA nerves. Bar graph reveals SOX2(+) nuclear quantification of WT (white bar) vs. 4OHT treated nerves (black bar); results ± SEM; $n = 3$ animals/group. WT nerves treated with 4OHT show approximately fourfold greater numbers of SOX2(+) nuclei ($P < 0.05$; Mann–Whitney *U* test). (*D*) Gross ON appearance (vehicle: Veh and experimental: 4OHT) of 34 d PN SOX2-DTA ONs 14 d posttreatment. 4OHT-treated ONs are modestly thinner (arrow) consistent with mild axonal loss, compared with vehicle-treated ONs. OT: optic tract. (*E–H*) TEM ultrastructure 14 d postinduction. (*E*) Anterior ON, 4OHT treated (1.5 mm from the posterior globe). Axons in the anterior 4OHT-treated ONs have reduced packing density, and increased extracellular vesicles, compared to vehicle ONs and more distal portion of the same nerve. The axon anterior segments have reduced myelination, compared to more distal segments. (Scale bars in *E* and *H*: 500 nm.) (*F*) Anterior ON, vehicle treated. (*G* and *H*) Distal ON, from *G*. 4OHT-treated SOX2-DTA and (*H*) vehicle-treated. Distal ON axons in both groups are closely packed, with dense myelination. (*I*) Mean axon diameter quantification of anterior and posterior ON segments from vehicle (white bars)- and 4OHT-treated (black bars) nerves ± SD. Myelinated axon diameters in the distal portions of SOX2-DTA animals treated with 4OHT (black bars) or vehicle (white bars) are similar in size distribution and myelin thickness. (*J*) Mean G ratios of vehicle (white bars)- and 4OHT-treated (black bars). ± SEM; $n = 3$ animals. A statistically significant increase in the G ratio of 4OHT-treated nerves occur in the anterior ON in animals treated 19 d postnatally, after local injection of 5 μL of vehicle or 4OHT ($P < 0.001$). Data from six random 164 μm^2 fields from each nerve region. NS: nonsignificant results in: Panel I (ONLR: $P = 0.8312$; optic nerve: $P = 0.8592$); Panel J (optic nerve: $P = 0.0545$). Two tailed *t* test.

Fig. 3*F*; vehicle treated). This was nonsignificant when multiple 168-μm^2 frames were compared from a number of animals (*SI Appendix*, Fig. S4).

Despite anterior ON hypomyelination, distal axon segment myelination was similar in both 4OHT- and vehicle-treated nerves (compare Fig. 3*G*; 4OHT-treated and Fig. 3*H*; vehicle-treated, respectively).

The presence of intraretinal SOX2(+) cells makes absolute isolation of the role of ONLR-NPCs problematic, since these cells could potentially contribute to ON development (37, 38). To determine whether intraretinal SOX2(+) NPCs contribute to late postnatal ONLR developmental function, we depleted retinal SOX2(+) cells in Sox2-Cre animals using intravitreal (IVT) injection of an AAV5-mCherry expression vector containing a

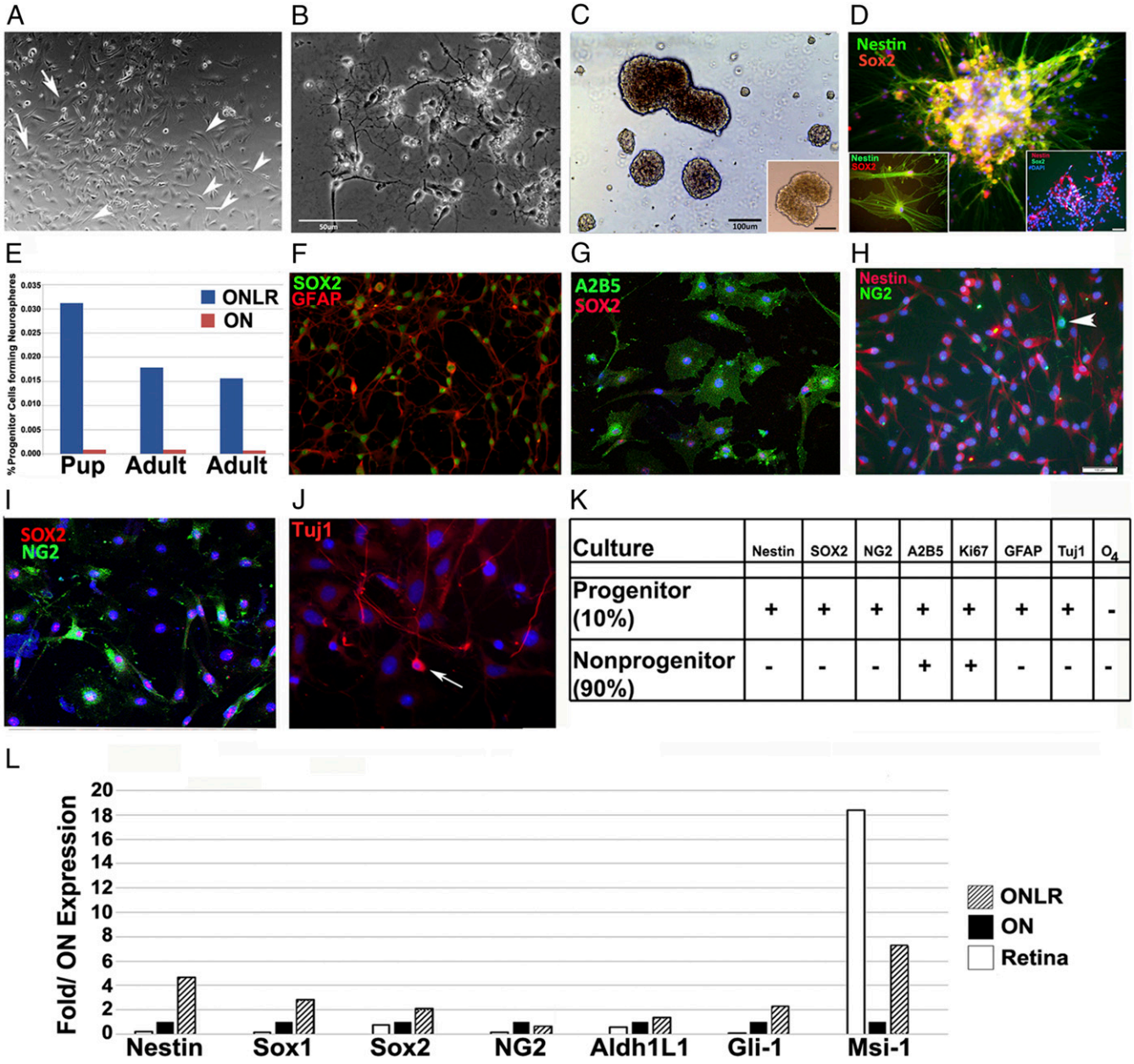

Fig. 4. Characterization of murine ONLR cell cultures and differential gene expression within the ONLR. (*A*) ONLR culture 6 d postisolation from 19 d/o mice. Arrowheads show cells consistent with NPC morphology. (*B*) ON culture 6 d postisolation. The majority of cells have extended processes consistent with oligodendrocyte and astrocytic morphology, and these cells are MBP(+) and GFAP(+), respectively. (*C*) ONLR-derived neurospheres. *Right Inset* shows SVZ-derived NS from the same animals for comparison. (Scale bar: 100 μm.) (*D*) ONLR-derived neurospheres regrown on adherent surface express NPC markers nestin (green) and SOX2 (red). *Left Inset*: individual ONLR-NPCs express both markers. *Right Inset*: nestin(+)/SOX2(+) SVZ-NPCs (arrows) grown under adherent conditions from the same animal. (*E*) Quantification of NS formation from pup (17 d old) and adult (60 d old) ONLR- and distal ON segments. NS formation ability is greatest in ONLR of both ages. (*F*) Cultured ONLR-NPCs express SOX2 (green) and GFAP (red). (*G*) SOX2 (red)/A2B5 (green) coexpression in ONLR culture. (*H*) ONLR nestin and NG2 expression. There is minimal colocalization and cells strongly expressing NG2 do not express nestin (arrowhead), suggesting that nestin(+) progenitors give rise to OPCs. (*I*) SOX2/NG2 expression in 1-mo cell cultures. NG2(+) (green) cells have multiple cytoplasmic projections, and SOX2(+) nuclei (red). A subpopulation of SOX2(+) cells are NG2(–). (*J*) Tuj1 (early neuronal) expression in 21 d ONLR cultures (arrow). (*K*) Expression characteristics table of the two main cell types found in nondifferentiated 30 d ONLR cultures (NPCs: 10% of cells; non-NPCs:90% of cells). ONLR-NPCs simultaneously express nestin, SOX2 and GFAP, while non-NPCs do not. (*L*) rqPCR of total RNA obtained from retina, ON, and ONLR of WT mice. ONLR expresses the highest level of nestin, Gli1, Sox1, and Sox2 of all three tissues, and there is increased Msi-1 expression relative to the rest of the ON.

floxed DTA gene driven by the EF1 promotor (39). AAV5 has in vivo affinity for astrocytes and NPCs, rather than neurons (40, 41). IVT AAV5 injections at 17 d PN generated mCherry expression in the inner retinal layer at 1 and 2 wk posttransfection (*SI Appendix*, Fig. S5 *A* and *B*, mCherry signal in green) Tamoxifen administration 2 wk posttreatment (beginning at PN31) reduced intraretinal SOX2(+) cells in the RGC layer by >50%, compared with treated WT animals (*SI Appendix*, Fig. S5); compare panels *SI Appendix*, Fig. S5*C* (WT) and *SI Appendix*, Fig. S5*D* (SOX-Cre). No hypomyelination was seen in the anterior ONs of SOX2-Cre-ERT2 heterozygotes transfected with AAV5-DTA compared to WT animals (*SI Appendix*, Fig. S6; compare TEMs of WT [*SI Appendix*, Fig. S6*A*] vs. SOX2-Cre ONs (*SI Appendix*, Fig. S6*B*); this was confirmed by the myelin G-ratio analysis (*SI Appendix*, Fig. S6*F*). DTA-AAV5 transfection at 17 d PN followed by early tamoxifen treatment 3 d later did not result in decreased anterior ON myelination, but also did not alter retinal SOX2(+) numbers in the RGC layer. Isolated loss of intraretinal SOX2(+) cells did not alter anterior ON myelination at any of the tested postnatal timepoints.

SOX2(+) NPCs are concentrated in the ONLR. Mouse ONLR and distal ON (>2 mm from the globe) from young (PN 20 d) and adult (60 d) animal were dissociated and cultured utilizing medium supplemented with FGF2 and grown on Matrigel. Cultivation without Matrigel resulted in poor growth from both laminar and ON cultures. Optimal propagation of ONLR cultures required concentrations of 10 to 15% Matrigel. Matrigel-supplemented ONLR cells initially formed flattened mixed-cell colonies (Fig. 4*A*) with two populations: A major population of fibroblast-type cells (~90%; Fig. 4*A*; arrows), and minor population (~10%) that were distinctly different, and which possessed an NPC-like appearance (Fig. 4*A*; arrowheads). The majority cell population, which are flattened, often stellate in appearance, are similar to those previously reported for human ONLR (42). Cultures generated from distal ON produced mainly cells morphologically similar to either oligodendrocytes (Fig. 4*B*) or astrocytes.

By immunohistochemistry, NPC-like cells were mitotically active by Ki67 immunoreactivity (*SI Appendix*, Fig. S7*E*). NPC-like cells coexpressed SOX2 and GFAP (Fig. 4*F* and also see *SI Appendix*, Fig. S7 *A–C*) and SOX2 and A2B5 (Fig. 4*G*), and nestin (Fig. 4*H*), but nestin(+) cells did not coexpress NG2 (Fig. 4*H*; arrowhead). Some SOX2(+) cells expressed NG2 (Fig. 4*I*), consistent with OPC expression. A few Tuj-1(+) cells were distinguishable in ≥21 d cultures (Fig. 4*J*). The ONLR NPC-like cells provided a continual source of astrocytes, distinguishable by their morphology and GFAP immunostaining. Along with astrocytes, we detected NG2(+)/nestin(−) cells (arrowhead, Fig. 4*H*). As nestin(+) cells gradually acquired NG2 expression, their nestin signal progressively declined. Our culture characterization results summary is shown as a table (Fig. 4*K*).

ONLR colonies derived from murine and human tissue grew under similar cell culture conditions and expressed markers in a similar fashion. For instances, colonies from mouse (Fig. 4*C*) and human (Fig. 5*G*) tissue formed neurospheres in low adhesion medium from the second passage onward. Neurospheres regrown on coated plates developed cells with fine processes, which coexpressed nestin and SOX2 (Fig. 4 *D*, *Left Inset*), similar to cells from human subventricular zone (SVZ)-derived neurospheres (Fig. 4 *D*, *Right Inset*) (43).

The loss of nestin in NG2(+) cells, coupled with the enhanced ability of ONLR cultures to form neurospheres suggested that ONLR-nestin(+)/SOX2(+) cells are distinct from the NG2(+)-OPC population, but capable of giving rise to SOX2(+)/NG2(+)OPCs. This observation is important because it suggests that ONLR-nestin expressing cells are at a more primitive progenitor stage than OPCs.

Sox2/nestin/GFAP(+) ONLR-derived cells thus represent a distinct NPC population potentially giving rise to all glial cell types, including OPCs. ONLR cultures supplemented with 10% fetal bovine serum (FBS) generated either GFAP(+) astrocyte-type cells or O_4(+) membranous oligodendrocyte-type cells (*SI Appendix*, Fig. S8*B*). ONLR-derived NPCs are thus progliogenic, with the propensity to differentiate into macroglia.

We performed lineage tracing in culture using ONLR cells derived from SOX2-Cre double mutant mice, induced with 5 mM 4OHT vs. vehicle. We compared GFP coexpression with Nestin (NPC marker), NG2, and A2B5 (OPC marker), MBP and Olig2 (oligodendrocyte markers), and GFAP (astrocyte marker) in undifferentiated ONLR cell cultures, and following either astrocytic or oligodendrocytic differentiation (see *Methods*). GFP(+)/nestin(+) cells gave rise to nestin (−)/GFP(+) cells of both astrocyte- and oligodendrocyte lineages.

ONLR- and ON-neurosphere forming ability was tested using second subculture passage-dissociated cells from both young and adult animals on a low adhesion surface. A total of 0.016 to 0.03% of ONLR cells in second passage cultures generated neurospheres (Fig. 4*E*; $n = 3$ experiments) that coexpressed the NPC markers nestin and SOX2 (Fig. 4 *D*, *Left Inset*). Distal ON cells generated fewer than one neurosphere per 10^6 cells (0.0007 to 0.0009%; Fig. 4*E*, red bars; $n = 3$ experiments). ONLR-neurospheres could be generated from both 17-d pups and mature (60-d) animals, but ONLR from mature animals generated fewer neurospheres compared with pups (Fig. 4*E*, compare blue bars in pup vs. adult). Immunohistochemical analysis of culture results are summarized in Fig. 4*K*.

We compared NPC-associated gene expression from adult mouse (60 d) retina, ONLR and ON tissues, and via rt-PCR (Fig. 4*L*). ONLR tissue expressed high nestin, Sox1-, and -2, and Gli-1 mRNA levels compared with ON or retina, and elevated Msi-1 mRNA levels compared with ON (Fig. 4*L*). Gli1 expression plays a key role in NPC-astrocyte progression, and early ocular development by interaction with the RGC-expressed morphogen sonic hedgehog (Shh) (44, 45). Msi1 is an NPC-expression marker (46).

Age-related quantitative changes in NPCs in rodent and human ONLR. Adult NPC numbers decline during aging (47), and ONLR-NPC decline may be associated with the aged ON's reduced reparative ability (48). A reduced capacity of cells from mature animals to generate neurospheres in vitro corresponded with our in vivo data showing reduced nestin expression and declining numbers of SOX2(+) cells in the ONLR of aged animals (Fig. 5*A*; 1 mo, and Fig. 5*B*, 24 mo). We performed a SOX2 nuclear count in ONLR and ON in mice of different ages (Fig. 5*C*). ONLR-SOX2(+) nuclear numbers declined 73% in 24 m/o animals, compared with 1 m/o animals (Fig. 5*C*, 24 mo; and black bars: 53 ± 36 vs. 197 ± 10; SEM; $n = 6$ nerves/group). Interestingly, ONLR has a greater number of SOX2(+) nuclei than distal ON, but the number of SOX2(+) cells in distal ON remains relatively constant during aging (Fig. 5*C*; white bars). ONLR thus exhibits an age-dependent decline in cells expressing NPC-associated markers.

The human ONLR contains an age-depletable NPC niche. The primate laminar structure is more elaborate than rodents (1), but the overall pattern of ONLR organization is similar in both phylogenetic families (5). Young human ONLRs strongly express filamentary nestin and possess abundant SOX2(+) nuclei (see *SI Appendix*, Fig. S9; fetal and 9 y/o human ONLR). Younger donors typically show increased SOX2(+) nuclear expression compared with tissue from older donors (compare Fig. 5*D*, 40 y/o, with Fig. 5*E*, 50 y/o, and Fig. 5*E* inset, 70 y/o). Donor tissues with prolonged times (>24 h) from demise until preservation showed reduced SOX2 signal (This is seen in *SI Appendix*, Fig. S9*B*; compare with Fig. 5*D*, 40 y/o; <24 h). This time-dependent decline of SOX2 expression increased SOX2 signal variability between donors of similar ages. Nestin expression was found to be less dependent on time to preservation, possibly because structural proteins are more stable than nuclear factors. ONLR-nestin

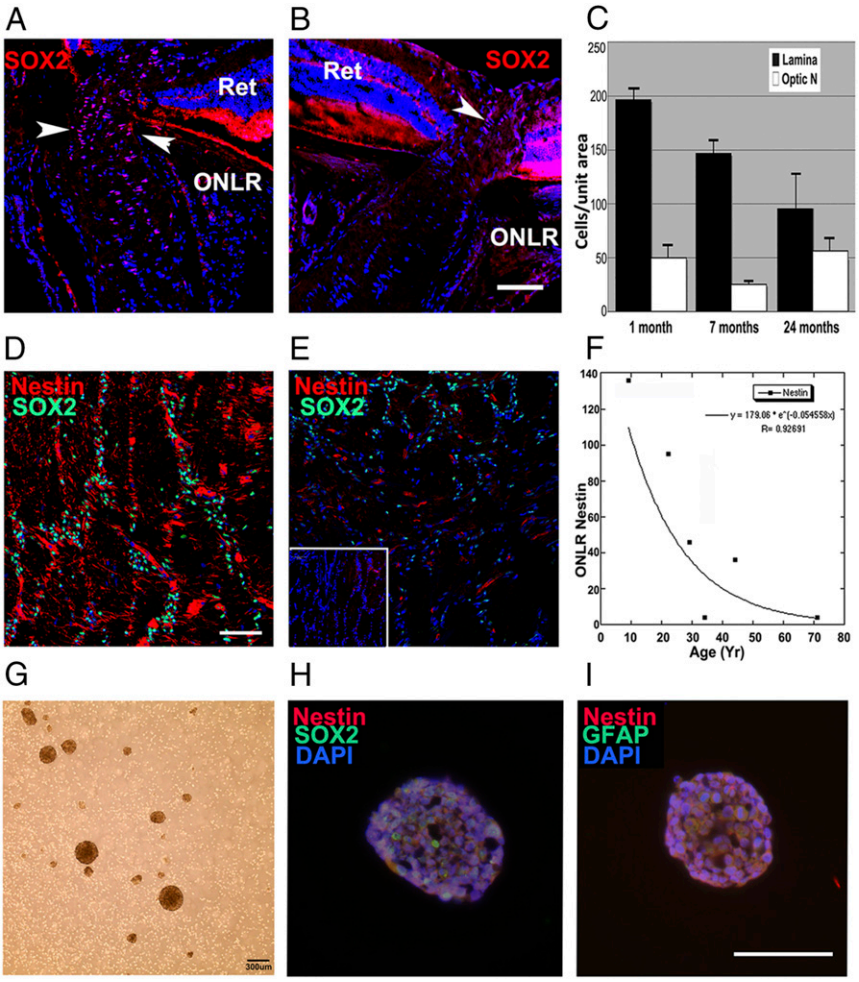

Fig. 5. Age-related NPC depletion in mouse and human ONLR and neurosphere development from human donors. (*A*) SOX2 nuclear expression (red) in a 6-mo mouse ONLR. Nests of SOX2(+) nuclei are present in the ONLR and anterior ON (arrowheads). (*B*) SOX2 nuclear expression in a 2 y/o mouse ONLR. There are fewer SOX2(+) nuclei (arrowhead), and SOX2(+) signal intensity is reduced. (Scale bar: 50 μm.) (*C*) SOX2 nuclear quantification in mouse ONLR and ON during aging. SOX2 nuclei declined 73% from 1 mo to 2 y (black bars) while SOX2 nuclear numbers in distal ON (white bars) remain relatively constant during this time ($n = 6$ nerves/group; data ± SEM). (*D* and *E*) Analysis of human ONLR-nestin and -SOX2 expression, with SOX2 immunostaining (green) and Nestin (red). (*D*) Forty y/o ONLR. Filamentous nestin expression is present, with numerous SOX2(+) nuclei. (Scale bar: 100 μm.) (*E*) Fifty y/o ONLR. There is reduced filamentous nestin expression, with remaining nestin present almost exclusively in the vasculature, and greatly reduced SOX2(+) nuclei. *Inset*: 71 y/o ONLR. The elderly ONLR reveals both a total lack of filamentous nestin and an absence of SOX2(+) nuclei. (*F*) Densitometric analysis of age-related human ONLR nestin expression. Nestin expression declines linearly from 9 y/o to 45 y/o, with severe loss in individuals >50 y of age. Donor history is shown in *SI Appendix*, Table S1A. (*G*) Human ONLR neurosphere formation (33 y/o donor). (*H*) SOX2 (green)/nestin (red) Immunolabeling of human neurosphere from culture shown in *G*. Individual cells express both SOX2 and nestin. (*I*) Nestin (red)/GFAP (green) expression in human neurosphere. Nestin and GFAP colocalize in individual cells. (Scale bar: 100 μm.)

expression declined precipitously with donor age [compare signals from youngest donors: with reduced signal from tissues of intermediate age donors 40 y/o (Fig. 5*D*) and 50 y/o (Fig. 5*E*)]. Filamentous nestin was absent in the ONLR of the oldest donors (Fig. 5*E Inset*). Human ONLR-nestin expression declined >90% by age 60 y (Fig. 5*F*, densitometric analysis: linear regression statistic, $r = 0.92$, Fig. 5*F*; the list of donor tissues is shown in *SI Appendix*, Table S1*A*). Tissue from elderly donors, even those having minimal time from collection to preservation contained few, if any ONLR-SOX2(+) nuclei or nestin (see 71 y/o ONLR in *Inset*, Fig. 5*E*). These data suggest that the human ONLR, like mice, contains an age-depletable cell niche of ONLR-NPCs.

To confirm the presence of human ONLR-NPCs, we dissociated ONLRs from freshly obtained human surgical specimens (approved by the University of Maryland, Baltimore institutional review board [IRB]). Human cultures utilized media conditions identical to those used for mouse ONLR cultivation (donor information shown in *SI Appendix*, Table S1B). Growth on adherent plates with Matrigel-coated surface generated mixed cultures, similar to those seen in rodent. Cells with a bipolar morphology were a prominent feature in early passage cultures grown on adherent plates. Neurospheres were generated when cells were regrown in low adherence conditions (Fig. 5*G*). Immunostaining of passage 3 human ONLR-neurospheres yielded cells coexpressing SOX2, GFAP, and nestin, consistent with NPC characteristics (Fig. 5 *H* and *I*).

Discussion

Our study demonstrates that the rodent and human postnatal ONLR contains nestin (+)/SOX2(+)/NG2(−) NPCs that give rise to OPCs, oligodendrocytes, and astrocytes. A vascular plexus is a characteristic of NPC niches (13), and this structure is present within the ONLR. Self-replenishing neural-derived cells

found within a dedicated vascular plexus, giving rise to culturable neurospheres, expressing multiple stem cell marker proteins, capable of differentiating into multiple neural forms, and which are age-depletable, fulfill the criteria of adult NPCs. ONLR-NPCs are distinct from nestin (−)/NG2(+) ON-derived OPCs, which are distinguished by their relative inability to generate neurospheres, grow poorly in the current medium, and give rise mainly to oligodendrocytes. ONLR-NPC frequency is similar to that previously reported hippocampus and white matter (28). The reduced ability of distal ON tissue to form neurospheres implies that cells in the distal ON have a lesser self-renewal capacity.

ONLR-NPCs resemble the "atypical astrocytes" previously reported to occur in the ONLR region (35). Lineage tracing of ON tissue in SOX2-Cre-ER2 X ROSA26 loxP(GFP) animals induced at 40 d PN (when the majority of ON growth is completed) and collected 30 d postinduction reveals few GFP(+)/CNPase(+) oligodendrocytes are present in the mid-ON, while both GFP(+)/CNPase(+) oligodendrocytes and GFAP(+) astrocytes are detectable in the anterior ON at this time point (*SI Appendix*, Fig. S1). We hypothesize that ONLR-NPCs perform multiple functions: During the early postnatal period, they may enable enhanced focal myelination in the growing axons as they emerge from the eye, producing directional (anterior > distal) myelination as well as generating astrocytes for the growing ON. In the mature ON, it is interesting to speculate whether ONLR-NPCs enhance cellular replacement from age- or stress-related loss and may also supply specific growth factors needed for normal axonal survival and function, similar to that seen in other CNS niches (49).

The optic nerve head has been reported to be the source of retinal astrocytes during early postnatal development (50). ON astrocytes are already present at E18 and fully distributed by 14 d PN (50), prior to the time points investigated in the current study. While it is tempting to consider that the ONLR-NPC niche may function to replace retinal astrocytes lost during aging, confirmation of this hypothesis will require lineage tracing techniques and approaches that are beyond the scope of the present report.

Postnatal axonal growth can occur at specific stress points located at myelinated:unmyelinated junctions (4). Since the region adjacent to the ONLR is where RGC axonal myelination begins, our results lead us to hypothesize that postnatal ON growth occurs by axonal extension from the unmyelinated retina, with myelination directly associated with emergence from the ONLR. ONLR-SOX2(+) NPCs can provide a source of oligodendrocytes and astrocytes during the period of intensive postnatal ON growth. Without adequate NPCs, axons may remain hypomyelinated. Our data show that the postnatal loss of SOX2(+) NPCs results in anterior hypomyelination. However, deciphering the role of ONLR-SOX2(+) NPCs is complicated by the presence of intraretinal SOX2(+) cells [both SOX9/SOX2(+) retinal NPCs and ChAT(+)/SOX2 amacrine cells], which could potentially contribute to ON growth. While our data are suggestive that ONLR-NPCs are associated with anterior ON myelination during growth, our studies evaluating postnatal ON growth were confined to the first 5 wk after birth, based on data showing skull growth around the ON reaches >95% of adult size by 36 d PN (51). AAV5-driven Cre expression resulted in depletion of retinal SOX2 expressing cells (*SI Appendix*, Fig. S5), without altering anterior ON myelination (*SI Appendix*, Fig. S6). Nevertheless, our current technology cannot completely rule out the possibility that retinal NPCS may contribute to early anterior myelination, since AAV-driven retinal SOX2 elimination was not completed before the majority of ON growth has occurred. Nevertheless, it is tempting to consider that postnatal ONLR-NPCs may be responsible for anterior ON myelination in the growing nerve. This is an area for future study.

The increased ratio of SOX2(+) nuclei to ONLR total nuclei in 2 m/o adult mice, vs. the distal ON, is maintained through at least 7 mo of age. Supporting these findings, the mouse ONLR formed neurospheres at a much higher frequency compared with distal ON tissue (graph, Fig. 4*E*). The ONLRs ability to form neurospheres was present in both young and adult animals, but neurosphere forming ability seems to decline in adult animals, compared with pups (graph, Fig. 4*E*, compare pup and adult ONLR). Neurosphere-forming ability is also present in ONLR from human donors. Our culture data confirm that that SOX2(+) cells in human and rodent ONLR-derived neurospheres coexpress nestin. These data support the hypothesis that the mammalian ONLR-SOX2(+)/nestin(+) cells represent a replicating NPC population, endowing the ONLR with a greater response repertoire than that of the distal ON.

Many NG2(+) cells were generated during ONLR-NPC culture, suggesting a preference for NPC > OPC differentiation. Terminal differentiation of cells from ONLR cultures generated both astrocytes and oligodendrocytes, with few (<3%) of NeuN(+) or Tuj1(+) cells. This is consistent with the ONLR-NPCs hypothesized role in glial replenishment. We confirmed this by ON immunohistochemistry following induction of SOX2-GFP double mutants, which yields GFP(+)/NG2(−) cells in the ONLR, and GFP(+) cells with both astrocytic and oligodendroglial cell morphology in the anterior ON, whereas GFP(+) cells in the distal portion of same nerves exhibit only either NG2(+) or oligodendrocyte morphology. These results support our hypothesis that one role for ONLR-NPCs is to enable in vivo generation of mature glia. Our experiments using more mature (40-d animals) suggests that following cessation of active ON growth, cells derived from ONLR-NPCs can migrate and give rise to mature oligodendrocytes, as well as GFAP(+) astrocytes, but this does not occur in more distal parts of ON.

In adults, overall oligodendrocyte generation declines, but the ONLR continues to have an increased Ki67(+) mitotic index (*SI Appendix*, Fig. S10), suggesting that the ONLR niche continues to contribute to adult glial cell replacement. We hypothesize that ONLR-NPCs have distinct roles during early postnatal and adult stages: during early postnatal development, ONLR-NPCs contribute glial cells for ON-axon growth, but in maturity contribute to glial cell replacement.

Both mouse and human ONLR-NPC numbers decline during aging. The loss of ONLR-NPCs in humans may alter the balance between degeneration and repair, contributing to the emergence of age-related ON diseases, such as OAG (52), a progressive ONLR-associated neuropathy. Progressive resistance to glaucoma treatment occurs in elderly individuals (53). ONLR-NPC depletion may contribute to OAG progression by reduced gliogenic support and associated neurotrophic factors important for RGC survival under stress, and which are secreted by cultured lamina-derived cells (54). We hypothesize that ONLR-NPCs present in younger individuals may be protective, and the age-related loss of ONLR-NPCs may contribute to disease progression via the inability to repair stress-related damage.

In summary, the ONLR in both humans and mice is not a nonproliferative barrier, but rather contains an NPC niche, which may have a role in both postnatal ON development and in adult ON support and repair. Age-related ONLR-NPC loss may contribute to ON diseases such as OAG. Understanding the roles of ONLR-NPCs may enable new therapeutic strategies to treat ON disease.

Methods

Statement on Data Sharing. Data deposited in Figshare: 10.6084/m9.figshare.12250223; 10.6084/m9.figshare.12250232; 10.6084/m9.figshare.12250241; 10.6084/m9.figshare.12251945; 10.6084/m9.figshare.12251957. ONLR-NPC cell culture aliquots will be provided on request along with the appropriate institutional approvals (IRB/IACUC) and materials handling fee.

Mouse Tissue Dissection. ON and ONLR were isolated from mice perfused with 4% paraformaldehyde-PBS (PFA), postfixed in 2% PFA, embedded in OCT medium, frozen at −80 °C, and sectioned at 10 μm.

Immunohistochemistry (IHC). Tissue sections were incubated with primary antibodies (listed in *SI Appendix*, Table S2) overnight at 4 °C, rinsed in PBS with 0.5% Triton X-100, incubated with appropriate secondary antibody for 1 h at 25 °C, DAPI counterstained, mounted, and examined via confocal microscopy using an Olympus E900 four channel microscope. Cell cultures were evaluated using a Nikon four channel fluorescent microscope.

Ki67 mitosis assay. Mouse ONLR cultures grown on 15% Matrigel were washed with D-PBS, fixed for 15 min with 4% PFA in PBS, reacted with Ki67 and SOX2 primary antibodies overnight at 4 °C, reacted with fluorescent-linked donkey secondary antibodies, DAPI stained, and examined using a Nikon fluorescent microscope.

Dissection ONLR and ON tissues for NPC cultivation. We enucleated eyes of appropriately aged mice with a 1.5 mm ON stump attached. Distal ON was obtained separately. Ten or more laminae were collected for NPC isolation. Tissues were placed into 300 μL cold Hibernate-A (GIBCO) until dissociation, and medium changed immediately prior to dissociation.

ONLRs were isolated and trimmed in a laminar flow hood following ON sheath removal. Human ONLRs were triturated using 2- to 29-gauge (ga) needles as knives. Distal ON was obtained from nerves separated from the ONLR by at least 2 mm, and triturated into smaller pieces using 29-ga needles.

ONLR-NPC and ON Cell Cultivation. Plates were coated with 15% Matrigel (VWR/Corning) diluted in Dulbecco's modified Eagle medium (DMEM) for a minimum of 1 h prior to use. Unbound Matrigel was aspirated, and 200 μL of complete NT-2 medium (see below) added per well of a 24-well plate.

Prior to cell dissociation, Hibernate-A was discarded and replaced with Dulbecco's complete PBS (DPBS) containing penicillin/streptomycin. ON/ONLR tissues were placed on ice for 5 min, centrifuged at 300 × *g* for 3 min, and washed twice with fresh DPBS. A total of 300 μL of collagenase (GIBCO; 1 mg/mL in sterile DPBS) was added and incubated at 37 °C, for 10 to 15 min, depending on the degree of tissue digestion. Tissues were homogenized by trituration 10 to 15 times through a 0.8-mm fire-polished Pasteur pipette. Five additional minutes at 37 °C was allowed for digestion if required. An equal volume of complete NT2 medium was then added to the tubes, centrifuged at 300 × *g* for 5 min, and supernatant discarded. Pellets were resuspended in 1 mL of media, containing 0.5 μL/mL of fungizone (GIBCO). Dissociated cells were manually counted via a hematocytometer, plated onto Matrigel-coated plates, and incubated in a humidity-controlled incubator at 37 °C supplemented with 5% CO_2 and 5% O_2. Final volume in each well was ∼500 μL. Cells were supplemented with 250 μL/well additional fresh complete NT2 medium every 2 to 3 d thereafter.

Immunocytochemistry (ICC). Plated cells were rinsed with DPBS, fixed in 4% PFA, rinsed with DPBS-0.05% Triton (DPBST), incubated with primary antibody at 4 °C overnight, and reacted with appropriate secondary antibodies for 1 h at RT (1:500 dilution), then washed, DAPI stained, and imaged.

GFP Induction and Differentiation of SOX2-Cre × ROSA26 tdTomato-loxP (GFP) Double Mutant Cells. ONLR cultures were induced with 5 mM 4OHT for 3 d. Cultures were then differentiated into either astrocytes (DMEM/F12 supplemented with 1% N2, 2 mM glutamax, 1% FBS) or oligodendrocytes (neurobasal medium supplemented with B27, glutamax and T3). Cultures were kept in differentiation medium for 5 to 7 d.

Neurosphere Immunostaining. Neurosphere (NS) formation was generated from second passage mouse ON/ONLR/SVZ stem cells grown on 15% Matrigel to 70% confluency. Cells were transferred to a 50-mL tube. An equal volume of fresh NT2 media was added to the tube and cells were redistributed evenly in the media by gentle aspiration. Cells were transferred to an Ultra-Low Attachment Surface 6-Well Plate (CORNING cat. no. 3471 Costar), with 500 μL of NT2 media. NS formation was observed between 4 to 7 d, imaged, and NS counted. NS were collected, briefly fixed in 4% PFA-PBS, cryoprotected in 30% sucrose, fixed in OCT at −80 °C, and sectioned at 10 μm.

Transgenic Animal Studies. All experimental protocols and procedures with mice were approved by Institutional Animal Care and Utilization Committee (IACUC; Baltimore, MD). Mice of both genders were used, kept on a 12-h light/dark cycle, with access to food and water ad libitum. Appropriate strains were mated and tail DNA was analyzed using recommended (Jax) gene-specific PCR primers to ensure genotypes. Nonmutant mice of the same background were used as controls.

B6.129(Cg)-Gt(ROSA)26Sortm4(ACTB-tdTomato,-EGFP)Luo/J (Jax Cat 007676); referred to ROSA-GFP) mice were crossed with B6;129S-Sox2tm1(cre/ERT2)Hoch/J (Jax Cat 017593) (referred to as SOX2-Cre). SOX2-Cre mice express Cre in all SOX2(+) cells. TAM and 4OHT bind to the ERT2 cassette to generate active Cre. B6.129P2- Gt(ROSA)26Sortm1(DTA)Lky/J (Jax Cat 009669; referred to as ROSA-Cre) contain a floxed diphtheria toxin antigen-A (DTA) in the ROSA26 locus. DTA expression occurs only in the presence of active Cre. Genotyped double-mutant progeny were generated for experimental procedures. These were referred as SOX2-GFP mice and SOX2-DTA mice. SOX2-Cre mice were used for AAV5 transfection experiments.

AAV-DTA construct and intravitreal injections. We eliminated SOX2(+)/ChAT (amacrine neurons) and SOX2/SOX9 (astrocyte) nuclei in the RGC layer, using an AAV vector serotype 5 construct mCherry-FLEX-DTA (39), (referred to as AAV5-Flex-DTA), which contains a FLOXed DTA gene but which expresses mCherry in all transfected cells, enabling determination of transfection efficiency. Only cells expressing active Cre induce DTA in transfected cells and are eliminated (39). AAV5 serotype has in vivo gliogenic, rather than neurogenic affinity. WT and SOX2-Cre animals were intravitreally injected with 2 μL of 1×10^{10} IU/mL strong mCherry expression was present throughout the RGC/astrocyte cell layers at 1- and 2-wk postintravitreal injection (*SI Appendix*, Fig. S5 *A* and *B*). We utilized two different SOX2 retinal elimination strategies: 1) Intravitreal injection with AAV5-Flex-DTA at 17 d, TAM at 21 d, and killed 14 d later. 2) Intravitreal injection with AAV5-Flex-DTA at 35 d, TAM treatment at 42 d, and killed 14 d later.

Only one anti-SOX9 antibody type (rabbit) was found to effectively label retinal astrocyte nuclei. Retinal sections were reacted with a mixture of either anti-SOX2/SOX9 (rabbit) primary antibodies to identify intraretinal astrocytes, or anti-SOX2/ChAT (rabbit) primary antibodies to identify amacrine neurons.

TAM and 4OHT treatment. TAM (systemic) or 4OHT (retrobulbar) injections activate Cre-ER2 recombination. TAM is a prodrug requiring liver metabolism to generate the active (4OHT) form. A total of 20 mg/kg of TAM (Sigma) was injected 4× over 5 d; 4OHT (Cayman) was prepared as a 30-mg/mL suspension in Kolliphor (Sigma). Five microliters of this mixture was injected behind the eye (RB injection).

Mouse injection and tissue harvesting schedule. TAM and 4OHT injections were performed on 19 d PN SOX2-DTA mice. Animals were killed 14 d postinjection. The 60 d mice were injected and killed at 14 d or 30 d postinjection. Tissue was also collected from WT adult mice at 2, 6, 12, and 24 mo of age.

SOX2-DTA mice. Systemic TAM is routinely fatal within 10 d in SOX2-DTA mice, due to global stem cell suppression (5/5 19d PN mice injected SC). Thus, we utilized local (RB) 4OHT administration. Animals were injected unilaterally with 4OHT, and the contralateral side with vehicle (Kolliphor)/internal control.

Human ONLR dissections and stem cell cultivation. All human specimens were obtained following UMB-Medical Center institutional review board (IRB) approved exemption for anonymized tissue for scientific use. Informed consent was not required. Eye tissues used for this purpose was stripped of identifiable information except for sex and age (*SI Appendix*, Table S1A). Tissues for immunohistochemistry and cultivation were obtained from a commercial donor source (Lions Eye Institute for transplant and research; Tampa, FL). Tissues for cultivation tissues were obtained from donors enrolled in the living legacy foundation (LLF; Halethorpe, MD), and from freshly isolated postsurgical specimens enucleated for severe, irreparable damage without hope of recovery, to prevent development of contralateral eye sympathetic ophthalmia (*SI Appendix*, Table 1). Postsurgical tissues were taken directly from the operating room on ice. Times from enucleation to final cultivation were ≤3 h.

Tissues were immersed 2× in 5% povidone iodine-DPBS solution and washed twice in sterile DPBS. ON and ONLR were located and carefully dissected from the globe, using a sterile microscissors. A total of 5 mm of adjacent nerve emerging from the globe was used for ONLR isolation, following optic nerve sheath and surrounding scleral wall removal. The anterior 2 mm of the retina entering the scleral wall was excised. Intact ONLR was placed into 1 mL of ice-cold sterile Hibernate-A medium, triturated, and centrifuged at 300 × *g* for 5 min. Media was discarded and replaced with DPBS containing penicillin/streptomycin at 0 °C for 5 min. Tissues were briefly centrifuged, DPBS solution was discarded, and washed twice with DPBS. One milliliter of collagenase (1 mg/mL in sterile DPBS was added, and tissue manually retriturated, and reincubated at 37 °C, for 15 to 20 min (dependent on state of tissue digestion).

Following further tissue dissociation, tissues were reincubated for 10 min at 37 °C. An equal volume of complete NT2 medium was added, centrifuged

at 300 × *g* for 5 min, and pellets were resuspended in 2 mL of NT2 medium containing 0.5 μL/mL of fungizone. Cells were plated onto 15% Matrigel coated six-well plates, and incubated at 37 °C in 5% CO_2.

Human ONLR neurosphere formation. Human ONLR cells grown to 70% confluence were subcultured (SC). SC2 cells were detached using a cell scraper, evenly redistributed, and transferred onto Ultra-Low Attachment Surface 10-cm Plates (Corning).

RNA isolation from eye tissues and cultures. Total RNA isolation was followed by genomic DNA removal and RNA clean up using the Qiagen RNeasy micro kit (Qiagen). ONLR and ON RNA were isolated from a minimum of 10 pooled samples (five animals/prep).

Real time quantitative PCR (qPCR). First strand cDNA synthesis was generated using the Invitrogen SuperScript First-Strand synthesis system with random primers. qPCR was performed using iQ SYBR Green Supermix (Bio-Rad) on an iCycler (Biorad). qPCR reactions contained 1× SYBR Green Supermix, 400 nM gene specific primers and various amounts of first strand cDNA, diluted to 1:10 in water depending on the abundance of the gene tested. Gene-specific primers were obtained from IDT (primer information: see *SI Appendix*, Table S3), qPCR reactions were performed on the following parameter: 95 °C/5 min initial denaturation, followed by 40 cycles of denaturation at 95 °C/30 s, annealing at 60 °C for 30 s, extension at 72 °C for 30 s, and a final 5-min extension. Only reactions yielding a single melting curve were used in the quantitative analysis. The ΔΔCt method of comparing relative sequence abundance was utilized, employing two internal control genes for quality, consistent with Minimum Information for Publication of Quantitative Real-Time PCR Experiment guidelines. All assays were run in duplicate.

Fluorescein-linked BSA (FITC-BSA) vascular imaging. This was performed as previously described (55). Tissues were imaged using a Zeiss two-photon microscope to a depth of 500 μm.

G ratio via transmission electron microscopy. Ocular tissues were isolated from transcardially perfused (2% PF-PBS) mice, and postfixed in buffered fixative containing paraformaldehyde and glutaraldehyde. Tissues were stained with uranyl acetate, embedded in Epon, and cross-sectioned at 200 nm. Anterior ON region 1.5 mm from the globe (avoiding the ONLR), and distal ON 4 mm from the globe were imaged with a Tecnai transmission electron microscope at 2,100× and 4,400×. G-ratio quantification (relative axonal myelination) was performed by outlining inner (axon) and outer (axon + myelin) axon using 4,400× micrographs. G ratios were evaluated from 200 ON axons/nerve.

ACKNOWLEDGMENTS. This work was supported by NIH R01-EY015304 to S.L.B., the Maryland Stem Cell Research Fund to R.J.F., and unrestricted funds from the Donner Foundation and the Holt Fund. The authors thank the Living Legacy Foundation of Maryland for providing human donor tissue samples. S.L.B. thanks Drs. Jeffrey Goldberg (Stanford University), and Adam Puche (University Maryland, Baltimore) for helpful suggestions concerning the DTA-NPC knockout experiments. This work utilized an EM sample preparation instrument that was purchased with funding from a National Institutes of Health shared instrumentation grant (1S10RR26870-1). The technical expertise of C. Charniga (Neural Stem Cell Institute), J. Strong and Dr. R.-C. Shi (Ultrastructure core, University of Maryland, Baltimore) is greatly appreciated.

1. S. L. Bernstein, M. Meister, J. Zhuo, R. P. Gullapalli, Postnatal growth of the human optic nerve. *Eye (Lond.)* **30**, 1378–1380 (2016).
2. P. C. R. Hughes, J. M. Tanner, J. P. G. Williams, A longitudinal radiographic study of the growth of the rat skull. *J. Anat.* **127**, 83–91 (1978).
3. A. Setzu, C. Ffrench-Constant, R. J. Franklin, CNS axons retain their competence for myelination throughout life. *Glia* **45**, 307–311 (2004).
4. J. L. Goldberg, How does an axon grow? *Genes Dev.* **17**, 941–958 (2003).
5. C. Albrecht May, Comparative anatomy of the optic nerve head and inner retina in non-primate animal models used for glaucoma research. *Open Ophthalmol. J.* **2**, 94–101 (2008).
6. C. Ffrench-Constant, R. H. Miller, J. F. Burne, M. C. Raff, Evidence that migratory oligodendrocyte-type-2 astrocyte (O-2A) progenitor cells are kept out of the rat retina by a barrier at the eye-end of the optic nerve. *J. Neurocytol.* **17**, 13–25 (1988).
7. J. V. Nguyen *et al*., Myelination transition zone astrocytes are constitutively phagocytic and have synuclein dependent reactivity in glaucoma. *Proc. Natl. Acad. Sci. U.S.A.* **108**, 1176–1181 (2011).
8. E. A. Nagelhus *et al*., Aquaporin-4 water channel protein in the rat retina and optic nerve: Polarized expression in Müller cells and fibrous astrocytes. *J. Neurosci.* **18**, 2506–2519 (1998).
9. J. M. Olver, A. C. McCartney, Orbital and ocular micro-vascular corrosion casting in man. *Eye (Lond.)* **3**, 588–596 (1989).
10. J. C. Morrison, E. C. Johnson, W. O. Cepurna, R. H. Funk, Microvasculature of the rat optic nerve head. *Invest. Ophthalmol. Vis. Sci.* **40**, 1702–1709 (1999).
11. C. A. May, E. Lütjen-Drecoll, Morphology of the murine optic nerve. *Invest. Ophthalmol. Vis. Sci.* **43**, 2206–2212 (2002).
12. Q. Shen *et al*., Adult SVZ stem cells lie in a vascular niche: A quantitative analysis of niche cell-cell interactions. *Cell Stem Cell* **3**, 289–300 (2008).
13. V. L. Bautch, Stem cells and the vasculature. *Nat. Med.* **17**, 1437–1443 (2011).
14. M. Tavazoie *et al*., A specialized vascular niche for adult neural stem cells. *Cell Stem Cell* **3**, 279–288 (2008).
15. H. Zhang *et al*., Long-term expansion of human neural progenitor cells by epigenetic stimulation in vitro. *Neurosci. Res.* **51**, 157–165 (2005).
16. M. E. van Strien *et al*., Isolation of neural progenitor cells from the human adult subventricular zone based on expression of the cell surface marker CD271. *Stem Cells Transl. Med.* **3**, 470–480 (2014).
17. R. Gorris *et al*., Pluripotent stem cell-derived radial glia-like cells as stable intermediate for efficient generation of human oligodendrocytes. *Glia* **63**, 2152–2167 (2015).
18. A. A. Davis, S. Temple, A self-renewing multipotential stem cell in embryonic rat cerebral cortex. *Nature* **372**, 263–266 (1994).
19. X. Qian *et al*., Timing of CNS cell generation: A programmed sequence of neuron and glial cell production from isolated murine cortical stem cells. *Neuron* **28**, 69–80 (2000).
20. S. H. Kang, M. Fukaya, J. K. Yang, J. D. Rothstein, D. E. Bergles, NG2+ CNS glial progenitors remain committed to the oligodendrocyte lineage in postnatal life and following neurodegeneration. *Neuron* **68**, 668–681 (2010).
21. J. W. Rowland *et al*., Generation of neural stem cells from embryonic stem cells using the default mechanism: In vitro and in vivo characterization. *Stem Cells Dev.* **20**, 1829–1845 (2011).
22. H. Mi, B. A. Barres, Purification and characterization of astrocyte precursor cells in the developing rat optic nerve. *J. Neurosci.* **19**, 1049–1061 (1999).
23. S. G. Wohl, C. W. Schmeer, T. Friese, O. W. Witte, S. Isenmann, In situ dividing and phagocytosing retinal microglia express nestin, vimentin, and NG2 in vivo. *PLoS One* **6**, e22408 (2011).
24. A. V. Gilyarov, Nestin in central nervous system cells. *Neurosci. Behav. Physiol.* **38**, 165–169 (2008).
25. D. Matsushima, W. Heavner, L. H. Pevny, Combinatorial regulation of optic cup progenitor cell fate by SOX2 and PAX6. *Development* **138**, 443–454 (2011).
26. J. Morrison *et al*., Structure and composition of the rodent lamina cribrosa. *Exp. Eye Res.* **60**, 127–135 (1995).
27. M. H. Maurer, R. E. Feldmann Jr., H. F. Bürgers, W. Kuschinsky, Protein expression differs between neural progenitor cells from the adult rat brain subventricular zone and olfactory bulb. *BMC Neurosci.* **9**, 7 (2008).
28. X. Lojewski *et al*., Human adult white matter progenitor cells are multipotent neuroprogenitors similar to adult hippocampal progenitors. *Stem Cells Transl. Med.* **3**, 458–469 (2014).
29. T. D. Nguyen *et al*., Prolonged cultivation of hippocampal neural precursor cells shifts their differentiation potential and selects for aneuploid cells. *Biol. Chem.* **394**, 1623–1636 (2013).
30. L. C. Foo, J. D. Dougherty, Aldh1L1 is expressed by postnatal neural stem cells in vivo. *Glia* **61**, 1533–1541 (2013).
31. D. C. Lagace *et al*., Dynamic contribution of nestin-expressing stem cells to adult neurogenesis. *J. Neurosci.* **27**, 12623–12629 (2007).
32. H. Liang, S. Hippenmeyer, H. T. Ghashghaei, A Nestin-cre transgenic mouse is insufficient for recombination in early embryonic neural progenitors. *Biol. Open* **1**, 1200–1203 (2012).
33. T. C. Badea, Y. Wang, J. Nathans, A noninvasive genetic/pharmacologic strategy for visualizing cell morphology and clonal relationships in the mouse. *J. Neurosci.* **23**, 2314–2322 (2003).
34. M. Saito *et al*., Diphtheria toxin receptor-mediated conditional and targeted cell ablation in transgenic mice. *Nat. Biotechnol.* **19**, 746–750 (2001).
35. R. Wang, P. Seifert, T. C. Jakobs, Astrocytes in the optic nerve head of glaucomatous mice display a characteristic reactive phenotype. *Invest. Ophthalmol. Vis. Sci.* **58**, 924–932 (2017).
36. U. Bartsch, D. Montag, S. Bartsch, M. Schachner, Multiply myelinated axons in the optic nerve of mice deficient for the myelin-associated glycoprotein. *Glia* **14**, 115–122 (1995).
37. A. G. Kautzman *et al*., Sox2 regulates astrocytic and vascular development in the retina. *Glia* **66**, 623–636 (2018).
38. I. E. Whitney *et al*., Sox2 regulates cholinergic amacrine cell positioning and dendritic stratification in the retina. *J. Neurosci.* **34**, 10109–10121 (2014).
39. Z. Wu, A. E. Autry, J. F. Bergan, M. Watabe-Uchida, C. G. Dulac, Galanin neurons in the medial preoptic area govern parental behaviour. *Nature* **509**, 325–330 (2014).
40. M. A. Anderson *et al*., Required growth facilitators propel axon regeneration across complete spinal cord injury. *Nature* **561**, 396–400 (2018).
41. J. L. Furman *et al*., Targeting astrocytes ameliorates neurologic changes in a mouse model of Alzheimer's disease. *J. Neurosci.* **32**, 16129–16140 (2012).
42. M. R. Hernandez, F. Igoe, A. H. Neufeld, Cell culture of the human lamina cribrosa. *Invest. Ophthalmol. Vis. Sci.* **29**, 78–89 (1988).
43. M. C. Moe *et al*., A comparison of epithelial and neural properties in progenitor cells derived from the adult human ciliary body and brain. *Exp. Eye Res.* **88**, 30–38 (2009).
44. M. Furimsky, V. A. Wallace, Complementary Gli activity mediates early patterning of the mouse visual system. *Dev. Dyn.* **235**, 594–605 (2006).

45. G. D. Dakubo *et al*., Control of glial precursor cell development in the mouse optic nerve by sonic hedgehog from retinal ganglion cells. *Brain Res.* **1228**, 27–42 (2008).
46. H. Takeda, H. Koso, L. Tessarollo, N. G. Copeland, N. A. Jenkins, Musashi1-CreER(T2) : A new cre line for conditional mutagenesis in neural stem cells. *Genesis* **51**, 128–134 (2013).
47. J. M. Encinas *et al*., Division-coupled astrocytic differentiation and age-related depletion of neural stem cells in the adult hippocampus. *Cell Stem Cell* **8**, 566–579 (2011).
48. M. T. Malik *et al*., Factors associated with recovery from acute optic neuritis in patients with multiple sclerosis. *Neurology* **82**, 2173–2179 (2014).
49. P. Lu, L. L. Jones, E. Y. Snyder, M. H. Tuszynski, Neural stem cells constitutively secrete neurotrophic factors and promote extensive host axonal growth after spinal cord injury. *Exp. Neurol.* **181**, 115–129 (2003).
50. M. L. O'Sullivan *et al*., Astrocytes follow ganglion cell axons to establish an angiogenic template during retinal development. *Glia* **65**, 1697–1716 (2017).
51. A. M. Maga, Postnatal development of the craniofacial skeleton in male C57BL/6J mice. *J. Am. Assoc. Lab. Anim. Sci.* **55**, 131–136 (2016).
52. J. M. Lee *et al*., Baseline prognostic factors predict rapid visual field deterioration in glaucoma. *Invest. Ophthalmol. Vis. Sci.* **55**, 2228–2236 (2014).
53. L. Rossetti *et al*., Focusing on glaucoma progression and the clinical importance of progression rate measurement: A review. *Eye (Lond.)* **24** (suppl. 1), S1–S7 (2010).
54. W. S. Lambert, A. F. Clark, R. J. Wordinger, Neurotrophin and Trk expression by cells of the human lamina cribrosa following oxygen-glucose deprivation. *BMC Neurosci.* **5**, 51 (2004).
55. J. D. Nicholson *et al*., PGJ_2 provides prolonged CNS stroke protection by reducing white matter edema. *PLoS One* **7**, e50021 (2012).